The Astronomical Journal, 159:118 (9pp), 2020 March https://doi.org/10.3847/1538-3881/ab7006

Near-infrared Imaging of a Spiral in the CQ Tau Disk

Taichi Uyama[1,2,3], Takayuki Muto[4], Dimitri Mawet[5,6], Valentin Christiaens[7], Jun Hashimoto[8,9,10], Tomoyuki Kudo[9], Masayuki Kuzuhara[8], Garreth Ruane[6], Charles Beichman[1,2], Olivier Absil[11], Eiji Akiyama[12], Jaehan Bae[13,29], Michael Bottom[6], Elodie Choquet[14], Thayne Currie[9,15,16], Ruobing Dong[17], Katherine B. Follette[18], Misato Fukagawa[3], Greta Guidi[19], Elsa Huby[20], Jungmi Kwon[21], Satoshi Mayama[22], Tiffany Meshkat[1], Maddalena Reggiani[23], Luca Ricci[24], Eugene Serabyn[6], Motohide Tamura[3,8,21], Leonardo Testi[25], Nicole Wallack[26], Jonathan Williams[27], and Zhaohuan Zhu[28]

[1] Infrared Processing and Analysis Center, California Institute of Technology, 1200 E. California Boulevard, Pasadena, CA 91125, USA
[2] NASA Exoplanet Science Institute, Pasadena, CA 91125, USA
[3] National Astronomical Observatory of Japan, 2-21-1 Osawa, Mitaka, Tokyo 181-8588, Japan
[4] Division of Liberal Arts, Kogakuin University, 1-24-2, Nishi-Shinjuku, Shinjuku-ku, Tokyo, 163-8677, Japan
[5] Department of Astronomy, California Institute of Technology, 1200 E. California Boulevard, Pasadena, CA 91125, USA
[6] Jet Propulsion Laboratory, California Institute of Technology, 4800 Oak Grove Drive, Pasadena, CA, 91109, USA
[7] Monash Centre for Astrophysics (MoCA) and School of Physics and Astronomy, Monash University, Clayton Vic 3800, Australia
[8] Astrobiology Center, National Institutes of Natural Sciences, 2-21-1 Osawa, Mitaka, Tokyo 181-8588, Japan
[9] Subaru Telescope, National Astronomical Observatory of Japan, Mitaka, Tokyo, 181-8588, Japan
[10] Department of Astronomy, School of Science, Graduate University for Advanced Studies (SOKENDAI), Mitaka, Tokyo 181-8588, Japan
[11] Space Sciences, Technologies, and Astrophysics Research (STAR) Institute, Université de Liège, Liège, Belgium
[12] Institute for the Advancement of Higher Education, Hokkaido University, Kita17, Nishi8, Kita-ku, Sapporo, 060-0817, Japan
[13] Department of Terrestrial Magnetism, Carnegie Institution for Science, 5241 Broad Branch Road NW, Washington, DC 20015, USA
[14] Aix Marseille Univ, CNRS, CNES, LAM, Marseille, France
[15] NASA-Ames Research Center, Moffett Field, CA, USA
[16] Eureka Scientific, 2452 Delmer Street Suite 100, Oakland, CA, USA
[17] Department of Physics & Astronomy, University of Victoria, Victoria, BC, V8P 1A1, Canada
[18] Physics and Astronomy Department, Amherst College, 21 Merrill Science Drive, Amherst, MA 01002, USA
[19] ETH Zurich, Institute for Particle Physics and Astrophysics, Wolfgang-Pauli-Str. 27, 8093 Zurich, Switzerland
[20] LESIA, Observatoire de Paris, Université PSL, CNRS, Sorbonne Université, Univ. Paris Diderot, Sorbonne Paris Cité, 5 place Jules Janssen, F-92195 Meudon, France
[21] Department of Astronomy, The University of Tokyo, 7-3-1, Hongo, Bunkyo-ku, Tokyo 113-0033, Japan
[22] The Graduate University for Advanced Studies, SOKENDAI, Shonan International Village, Hayama-cho, Miura-gun, Kanagawa 240-0193, Japan
[23] Institute of Astrophysics, KU Leuven, Celestijnlaan 200D, B-3001 Leuven, Belgium
[24] Department of Physics and Astronomy, California State University Northridge, 18111 Nordhoff Street, Northridge, CA 91330, USA
[25] ESO/European Southern Observatory, Karl-Schwarzschild-Strasse 2, D-85748 Garching bei München, Germany
[26] Division of Geological and Planetary Sciences, California Institute of Technology, 1200 E. California Boulevard, Pasadena, CA 91125, USA
[27] Institute for Astronomy, University of Hawaii, Honolulu, HI 96822, USA
[28] Department of Physics and Astronomy, University of Nevada, Las Vegas, 4505 S. Maryland Parkway, Las Vegas, NV, 89154-4002, USA
Received 2019 September 3; revised 2020 January 17; accepted 2020 January 23; published 2020 February 21

Abstract

We present L'-band Keck/NIRC2 imaging and H-band Subaru/AO188+HiCIAO polarimetric observations of the CQ Tau disk with a new spiral arm. Apart from the spiral feature, our observations could not detect any companion candidates. We traced the spiral feature from the r^2-scaled High-Contrast Coronographic Imager for Adaptive Optics (HiCIAO) polarimetric intensity image and the fitted result is used for forward modeling to reproduce the ADI-reduced NIRC2 image. We estimated the original surface brightness after throughput correction in the L' band to be $\sim$126 mJy arcsec^{-2} at most. We suggest that the grain temperature of the spiral may be heated up to $\sim$200 K in order to explain both of the H- and L'-band results. The H-band emission at the location of the spiral originates from the scattering from the disk surface while both scattering and thermal emission may contribute to the L'-band emission. If the central star is only the light source of scattered light, the spiral emission at the L' band should be thermal emission. If an inner disk also acts as the light source, the scattered light and the thermal emission may equally contribute to the L'-band spiral structure.

Unified Astronomy Thesaurus concepts: Protoplanetary disks (1300); Coronagraphic imaging (313)

1. Introduction

Protoplanetary disks are good laboratories for understanding the relationship between planet formation and disk evolution mechanisms. Previous photometric/spectroscopic studies of young stellar objects (YSOs) with infrared (IR) excesses predicted gaps in their disks (transitional disk; Strom et al. 1989). As instruments have developed, high-spatial resolution observations with near-IR polarimetric imaging or (sub-)millimeter interferometry revealed more asymmetric disks with gaps (e.g., Hashimoto et al. 2012), rings (e.g., ALMA Partnership et al. 2015; Andrews et al. 2018), spirals (e.g., Muto et al. 2012; Benisty et al. 2015; Pérez et al. 2016; Huang et al. 2018; Uyama et al. 2018), dust traps (e.g., van der Marel et al. 2013), an asymmetric blob in the disk midplane (e.g., Tsukagoshi et al. 2019), and velocity kink in gas kinematics (e.g., Pinte et al. 2018). In particular, spiral arms are one of the most intriguing signposts of planet formation in the disk because a protoplanet behaves as a perturber of the disk, which can lead to spiral formation (Zhu et al. 2015; Dong et al. 2018b), but yet no confirmed connection between an observed spiral arm and a planetary mass companion has been made observationally (but see

[29] NHFP Sagan Fellow.

Table 1
Observing Logs

Instrument	Date (*UT*)	Observing Mode	Band	Total Exposure Time (s)
Keck/NIRC2	2018 Dec 24	ADI	L'	1800
Subaru/HiCIAO	2015 Dec 31	PDI[a]	H	540

Note.
[a] ADI was combined with PDI but we focus on only PDI reduction in this study (see Section 2.2).

Wagner et al. 2019). Gravitational instability in the disk can produce spirals (Dong et al. 2015a).

Radio continuum observations measure thermal emission of dust grains in the disk midplane and those at different excitations of gas such as CO(2−1) and CO(3−2) can probe the distribution of different layers of molecular gas species. Performing interferometric observation in radio wavelength enables the achievement of sufficient spatial resolution to resolve detailed asymmetric structure. High-contrast broadband imaging with a variety of differential imaging methods can sometimes detect intriguing disk features. Polarization differential imaging (PDI; Kuhn et al. 2001) provide polarimetric intensity (PI), which traces scattered starlight from the disk surface. Those explorations with angular differential imaging (ADI; Marois et al. 2008) for young planets, in parallel to disk studies, have not successfully detected the most convincing protoplanets within such disks until PDS 70b was reported recently (Keppler et al. 2018). The results of that paper support the theory that planets really form in protoplanetary disks. Interestingly, several L'-band observations successfully detected asymmetric disk features with ADI (e.g., HD 142527, HD 100546, and MWC 758; Rameau et al. 2012; Currie et al. 2015; Reggiani et al. 2018; Wagner et al. 2019). As Lyra et al. (2016) performed a 3D simulation and predicted that a high-mass planet can induce shocks and heat the spiral to a few hundred Kelvin (see Figure 4 in the paper), the L'-band observation has the capability to detect thermal emission from the disk. In the near future one can expect to discover more planets undergoing formation and further searches for asymmetric disk features as well as for protoplanets will help to understand the links between planet formation and disk evolution.

CQ Tau (R.A. = 05:35:58.47, Decl. = +24:44:54.1) is a YSO in the Taurus star-forming region (F2-type, $1.67 M_{\odot}$, ∼10 Myr, 162 pc; Natta et al. 2001; Gaia Collaboration et al. 2018; Ubeira Gabellini et al. 2019). C_I observations by the Atacama Pathfinder Experiment (APEX) and comparison with chemical models suggested that CQ Tau likely has a transitional disk (Chapillon et al. 2010). An Atacama Large Millimeter/submillimeter Array (ALMA) observation reported a large gap in the 1.3 mm continuum, ^{13}CO, and ^{18}CO (Ubeira Gabellini et al. 2019). The gap sizes in the dust and gas are estimated at 56 au and 20 au in radius, respectively. Ubeira Gabellini et al. (2019) also performed 3D numerical simulations and suggested an unseen protoplanet in the disk. To further search for protoplanets as well as asymmetric features in the CQ Tau disk, we used two high-contrast imaging observations with Keck/NIRC2 and Subaru/AO188+HiCIAO. Although we did not detect any companion candidates, we detected a spiral feature in the disk. In this study, we analyze the detected spiral feature and investigate the possible links to ongoing planet formation.

2. Observations and Results

We used two infrared data sets taken from Keck/NIRC2 and Subaru/AO188+HiCIAO. We also used an ALMA archival image, observed in Cycle 5 (ID: 2017.1.01404.S, PI: L. Testi), which achieved a noise level of ∼23 μJy beam^{-1} and a beam size of 69 and 51 mas for major axis and minor axis, respectively, for comparison with the infrared data. Details of this data set as well as other ALMA data of CQ Tau are described in Ubeira Gabellini et al. (2019). Table 1 summarizes the observing logs for both observations. Sections 2.1 and 2.2 describe each observation and its result. Section 2.3 compares both results.

2.1. Keck/NIRC2

CQ Tau was observed on UT 2018 December 24 (PI: D. Mawet) using the Keck/NIRC2 vortex coronagraph (Mawet et al. 2017; Serabyn et al. 2017; Xuan et al. 2018) combined with ADI. The observation achieved an angular rotation of ∼111°. No standard stars were taken in the same epoch and we did not conduct point-spread function (PSF) subtraction by reference differential imaging (RDI; Ruane et al. 2019) in this study. We measured the off-axis PSF and determined that the FWHM was 9.2 pix (∼0.″0915 with a pixel scale of 9.972 mas pix^{-1}). After a first reduction including flat-fielding, bad-pixel correction, sky-subtraction, and image registration, the data set was processed via the vortex image processing (VIP; Gomez Gonzalez et al. 2017)[30] package that applies a principal component analysis (PCA) for the ADI reduction (Amara & Quanz 2012; Soummer et al. 2012).

Figure 1 shows the Keck/NIRC2 ADI-reduced image of CQ Tau overlaid with the ALMA continuum (left) and Subaru/High-Contrast Coronographic Imager for Adaptive Optics (HiCIAO) PI (right; see Section 2.2 for the data). VIP produces a set of different principal components (PCs), results of which are shown in the Appendix. We adopted PC = 8 among these PCs for presenting our result because this image shows an extended object at separations between ∼0.″2 and 0.″4, and position angles (PAs) between ∼45° and 110° with a signal-to-noise ratio (S/N) ∼7–8. The feature appears robust because it survives for a wide range of PC values (see Figure 7). We marginally found some other sources (see Figure 7) in a set of ADI-reduced images, whose S/Ns fall less than 5 at a certain PC and do not discuss other companion candidates. We converted counts into the surface brightness using previous L'-band photometry (2.4 Jy for CQ Tau; McDonald et al. 2017) and the brightest region in this feature has 68 ± 8.5 mJy arcsec^{-2}. The VIP package enables one to set different fields of view (FoV) and inner working angles (IWA). We adopted IWA = 16 pix so that the asymmetric feature is reproduced with a higher S/N. We reran VIP by setting a smaller IWA to check whether other companion candidates appear at

[30] https://github.com/vortex-exoplanet

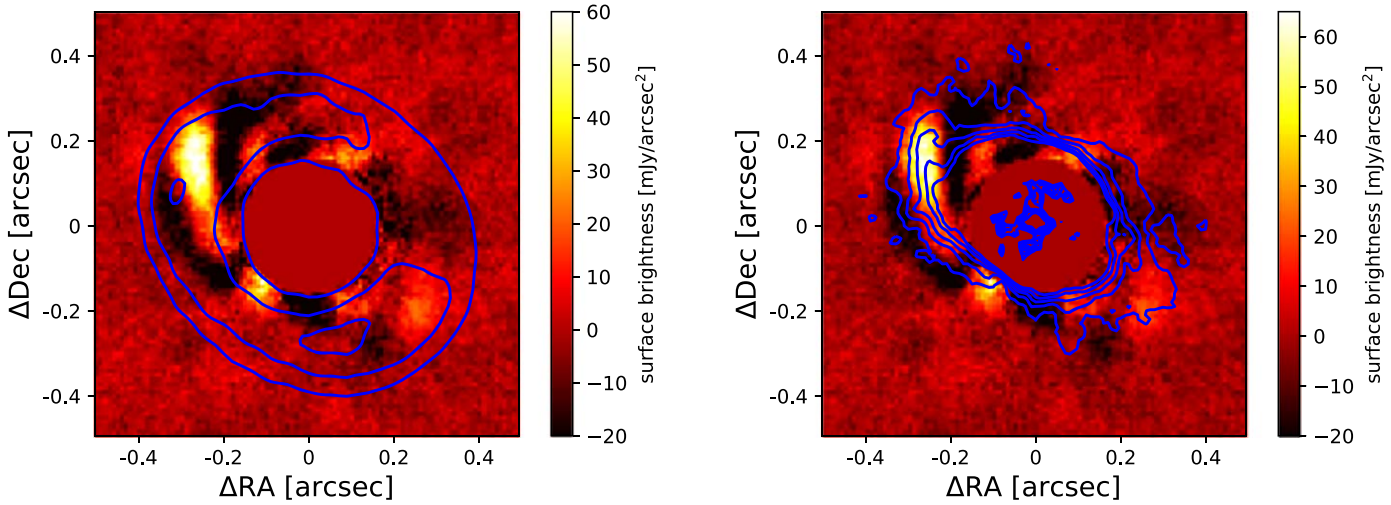

Figure 1. Left: Keck/NIRC2 L'-band image of CQ Tau overlaid with contours of the ALMA dust continuum image at 1.3 mm at 30, 50, and 70σ (1σ = 23 μJy beam^{-1}), respectively (blue). The central star is masked by the algorithm. North is up and east is left. The color scale shows surface brightness in mJy arcsec^{-2} unit. Right: same as the left figure except for the contours. The contours correspond to Subaru/HiCIAO H-band PI data at 10, 20, 30, 40, and 50 mJy arcsec^{-2}, respectively (blue).

separations smaller than 16 pix and confirmed that only residuals of speckles that vary among different PCs were shown. We first attempted to fit this extended object with a point-source Gaussian, which provided a poor match and thus we concluded that it corresponds to an asymmetric structure in the CQ Tau disk. Figure 2 shows a polar-projected image suggesting that this feature likely corresponds to a spiral. CQ Tau is one of only a few systems that have a spiral detected in the L' band (see Section 1 for the L'-band disks).

We then compared our results with the ALMA archival data. The spiral overlaps with the ring of the dust continuum, but the ADI-reduced signal experiences self-subtraction by the reduction algorithm as negative regions shown at both sides of the spiral. Centrosymmetric features in the CQ Tau disk are also removed by self-subtraction and thus cannot be seen in the ADI-reduced image (Milli et al. 2012).

Apart from the spiral feature, we did not detect any companion candidates within $\sim$0.″9 from the central star. The NIRC2 figure with a larger FoV is shown in the Appendix. We then calculated noise profiles as a function of separation relative to the signal from the central star. Figure 3 shows a 5σ detection limit of the NIRC2 data. Although the spiral feature affects the detection limit between 0.″2 and 0.″4, we achieved 2.9 $\times$ 10^{-5} at 0.″5. Compared with an evolutionary model (COND03; Baraffe et al. 2003) assuming 10 Myr, our contrast limit could constrain down to $\sim$5 M_J outside the spiral.

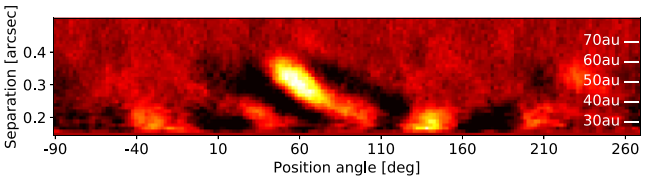

Figure 2. Polar-projected image of the NIRC2 image in Figure 1. We arrange the image starting at a PA of $-90°$ to show the spiral feature clearly.

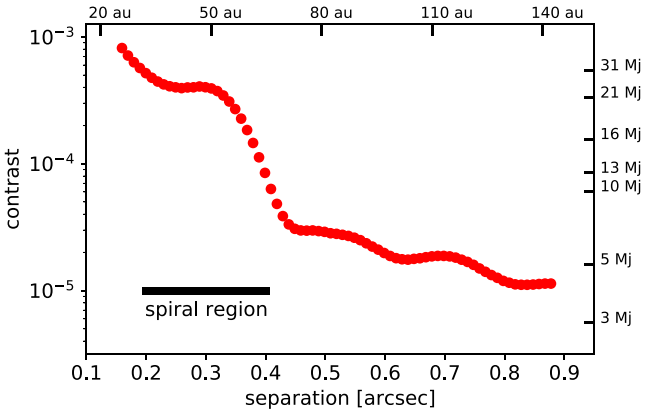

Figure 3. 5σ contrast limit of the NIRC2 image with PC = 8. We also plot the expected contrast of a substellar-mass object on the right using the COND03 model.

2.2. Subaru/HiCIAO

Subaru/AO188+HiCIAO observed CQ Tau in a combination of PDI and ADI as part of the Strategic Exploration of Exoplanets and Disks with Subaru (SEEDS) project (Tamura 2009). No coronagraph was used in this observation. The total exposure time of the HiCIAO data is only 9 min with FWHM = 5.3 pix ($\sim$50 mas with a pixel scale of 9.5 mas pix^{-1}), which achieved an inner working angle of $\sim$0.″77 after the ADI reduction and is insufficient for searching planets embedded in the CQ Tau disk (for the ADI result at separations $\geqslant$1.″0, see Uyama et al. 2017). In this study, we focus only on the PDI reduction. SEEDS adopted standard PDI (sPDI) and quad PDI, where a different number of Wollaston prisms was used, and sPDI was applied to CQ Tau's observation (for detailed information see Uyama et al. 2017). After the first reduction of destriping the HiCIAO pattern, flat-fielding, distortion correction, and image registration, we reduced the polarimetric data sets by means of an IRAF pipeline,[31] which was used in previous HiCIAO PDI studies (e.g., Hashimoto et al. 2011, 2012). Figure 4 shows the PI image of CQ Tau overlaid with the ALMA continuum. The whole disk cannot be

[31] IRAF is distributed by National Optical Astronomy Observatory, which is operated by the Association of Universities for Research in Astronomy, Inc., under cooperative agreement with the National Science Foundation.

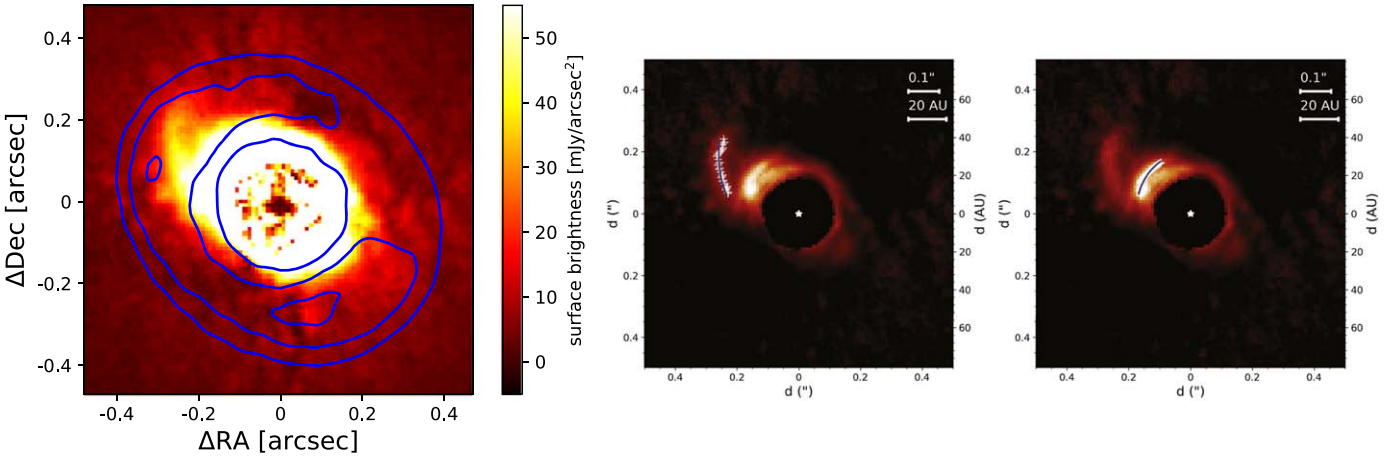

Figure 4. Left: PI image of the Subaru/HiCIAO *H*-band observation overlaid with the ALMA continuum. North is up and east is left. Middle: r^2-scaled PI image including the identified trace of the outer spiral (white crosses) and the best-fit logarithmic spiral (blue curve). Right: same, but for the inner (tentative) spiral. For estimating the pitch angle we used a further deprojected image.

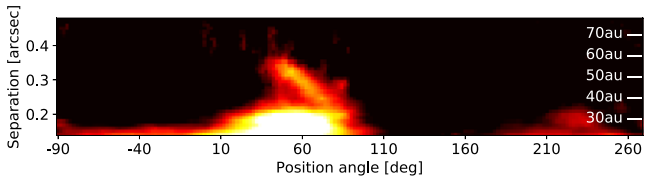

Figure 5. Same as Figure 2 but for the r^2-scaled HiCIAO PI image.

investigated since there are residual speckles that cannot be removed through post-processing due to short exposure time. We did not detect a gap in the surface of CQ Tau's disk. The PI image shows the spiral feature at the same location as shown in the NIRC2 image. In order to investigate the S/N of the spiral, we used perpendicular regions to the spiral whose PAs range from 125°–165°, 305°–345° for calculating a noise (defined as the standard deviation in the specified area) radial profile. We finally confirmed that the spiral has an S/N ∼5–6 in the PI image. There may be other disk features shown in the PDI-reduced image but below 5σ significance due to speckles in the inner region. An r^2-scaled PI image (see Figure 5 for a polar-projected image) clearly shows the spiral feature. There is another extended region at PAs between 10° and 90°, which is perhaps another asymmetric feature and possibly detected in the NIRC2 data with PC = 5, 8, and 10 in Figure 7 with insufficient significance. We discuss this inner feature in Section 2.3. We note that a gap-like feature close to the central star may be affected by r^2-scaling because the original HiCIAO data set does not show such a feature (see the left image in Figure 4 for the PI signal and the right image in Figure 1 for the contour).

2.3. Comparison of the Two Data Sets

In both observations we clearly detected the spiral feature, which overlaps with the ring structure in the millimeter continuum detected by ALMA. The presence of the spiral is consistent with a prediction of a ∼6–9 M_J planet at 20 au (Ubeira Gabellini et al. 2019). However, our observation could not achieve a sufficient contrast limit to detect/constrain such a faint protoplanet. We checked whether a counterpart of the spiral is shown in the ALMA gas data. Tang et al. (2017) reported a pair of spirals for AB Aur at ^{12}CO emission that correspond to the PI signal (Hashimoto et al. 2011). However, Ubeira Gabellini et al. (2019) did not show any clear spiral features in the ^{12}CO data.

The right panel of Figure 1 compares the NIRC2 and HiCIAO results and these shapes show a good agreement with each other. Polar-projected images (Figures 2 and 5) also clearly show that the spiral feature increases in distance from the central star. We note that the surface brightness in each band shows a different parameter. The NIRC2 and HiCIAO results correspond to the total intensity and polarimetric intensity, respectively. We discuss the difference between these results in Section 3.2. We measured the pitch angle based on the best-fit logarithmic spiral to the trace of the spiral. The trace was identified as radial maxima in azimuthal bins of 1° in the image obtained after deprojection using inclination and PA of the major axis derived by Ubeira Gabellini et al. (2019): $i = 35°$ and $\mathrm{PA}_a = 55°$. Since the spiral feature in the NIRC2 image experiences self-subtraction and is distorted by the reduction algorithm, we used only the HiCIAO data to measure the pitch angle. The PI data corresponds to scattering profiles from the disk surface and does not experience self-subtraction. The fitted result for the spiral (the middle panel in Figure 4) is 34° ± 2°. We also attempted to fit the extended inner region at PAs between 10° and 90°. The result is shown in the right panel of Figure 4 and the pitch angle is measured at 4° ± 3°. In addition to fits to the logarithmic spiral equation, we also fitted the spiral trace to the general Archimedean equation. The result is shown in the Appendix. We note that because scattered light originates from a cone-shape surface instead of a flat plane, when viewed at a finite inclination, different regions in the disk are compressed differently (e.g., Figure 4; Ginski et al. 2016). Because of this, a disk structure in surface density traced by millimeter continuum emission can be projected to a different location in scattered light (e.g., the southern spiral arm in MWC 758; Dong et al. 2018a). Simple deprojection by linearly expanding the disk along the minor axis by a factor of $1/\cos i$ generally does not perfectly restore the face-on view of the disk (Dong et al. 2016). Therefore, our measurements of the arm pitch angles are approximations only. Future modeling work is needed to simultaneously determine the shapes of the disk surface and the spiral arms.

We used both fit results to infer input parameters for the forward modeling of the L'-band feature (for the detailed method for the forward modeling, see Christiaens et al. 2019)

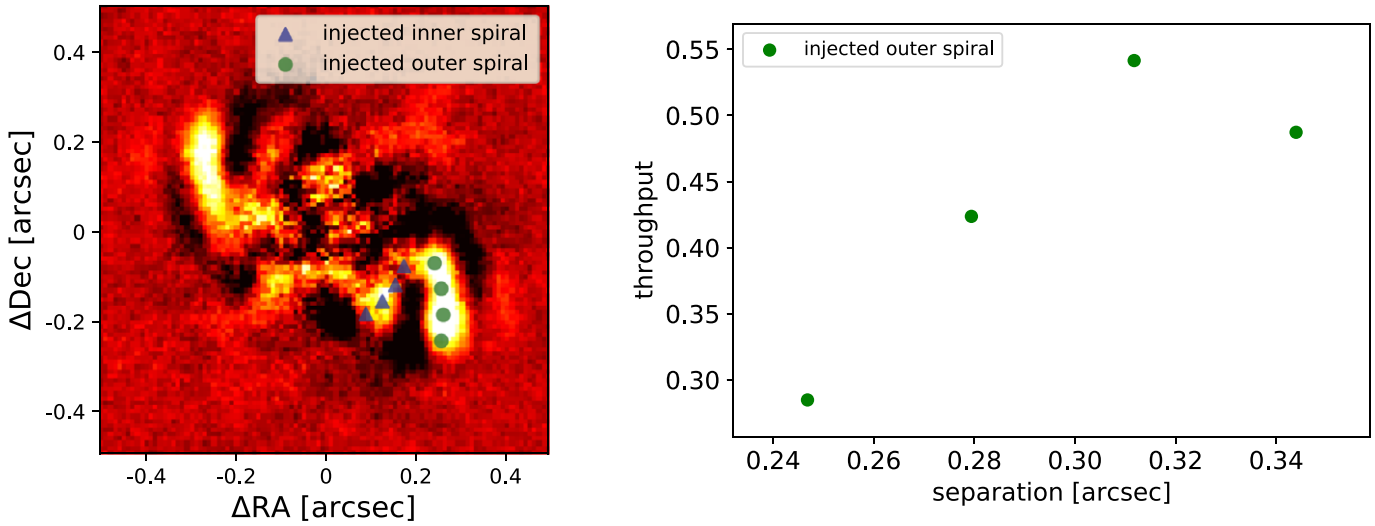

Figure 6. Left: VIP–PCA reduced image for the NIRC2 data with injected fake spirals at symmetric positions with respect to the center. Right: measured throughput of the injected outer spiral as a function of separation.

to measure a throughput (signal loss due to the ADI reduction); Figure 6 shows our result with injected spirals. We used the off-axis PSF of CQ Tau and injected fake PSFs at several separations and PAs to produce fake spiral features (injected positions are shown in Figure 6). We then measured the ratio between input flux and output flux at the injected locations, which is shown in the right panel of Figure 6. Our forward modeling reproduced the outer spiral with a flux recovered by a throughput of 0.54 at 50 au, which corresponds to 126 mJy arcsec^{-2} at the brightest region in the spiral. On the other hand, however, the injected inner spiral is largely affected (a throughput less than 0.3) by not only self-subtraction at small separations but also negative regions produced by the existence of the outer spiral. As the S/Ns of this feature in the practical NIRC2 and HiCIAO data are less than 5, we do not conclude that this inner feature is a spiral.

The CQ Tau disk has a striking similarity with the disk around V1247—both of which show one prominent arm in scattered light and a ringed disk in millimeter continuum emission (Ohta et al. 2016; Kraus et al. 2017). In addition, they share a similar inclination of ~30°–35°, and the major spiral arm seen is in the direction of the major axis. Simulations have shown that while a massive companion may induce a pair of nearly symmetric spiral arms, when viewed at a modest inclination one of the arms may be compressed more than the other in scattered light, thus falling inside the inner working angle (Dong et al. 2016). Future observations may push for inner separations to look for possible additional arms hidden under the current image mask.

3. Discussion

The spiral feature in the L' band may be reproduced by two scenarios; (1) the spiral is heated and self-luminous or (2) the surface of the spiral scatters the stellar light as shown in the Subaru/HiCIAO image. Hereafter we use the peak values at the spiral region as a representative surface brightness. The spiral feature extends over ~0.″2-scale, which is only a factor of ~2 larger than the angular resolution of the NIRC2 result. This prevents us from discussing the detailed spiral profiles of the surface brightness distribution.

3.1. Disk Temperature

We first investigate whether the L'-band emission can be reproduced by thermal emission from small grains. We assume that the disk is optically thick at the L' band. If the observed emission of 126 mJy arcsec^{-2} is entirely due to thermal emission from optically thick dust, the temperature of the grains is expected to be $T_{\rm grain} \sim 202.5$K.

Provided that small grains at the spiral absorb shorter wavelengths of stellar light and emit their heat at ~3–4 μm, the grain temperature is given by

$$(1-\omega_\nu)\pi a_{\rm grain}^2 \frac{L_\star}{r_{\rm spiral}^2} < Q_{\rm abs}(\lambda_\star) > = 4\pi a_{\rm grain}^2 \sigma T_{\rm grain}^4 Q_{\rm abs}(\lambda_{\rm grain}), \quad (1)$$

where $Q_{\rm abs}(\lambda)$ is the absorption efficiency at λ and $a_{\rm grain}$ is the size of the grain. With this equation, we can derive a set of dust size ($a_{\rm grain}$) and albedo (ω_ν) that can reproduce $T_{\rm grain} = 202.5$K. Here we assume $<Q_{\rm abs}(\lambda_\star)> = \frac{\int Q_{\rm abs} B_\lambda(T_\star) d\lambda}{\int B_\lambda(T_\star) d\lambda} \simeq 1$ for simplicity. This relation is compared with the model of astronomical silicate (Draine & Lee 1984). We find a set of $a_{\rm grain} \sim 0.8\mu$m and albedo~0.2 can reproduce $T_{\rm grain} = 202.5$ K and is consistent with the astronomical silicate model. The dust opacity (κ) per unit dust mass (assuming that the gas-to-dust ratio is 100) is also estimated to be 3.4×10^3 cm^2 g^{-1} and 1.1×10^3 cm^2 g^{-1} at the H and L' bands, respectively. With the small grain surface density of 0.0375 g cm^{-2} of CQ Tau's disk (Ubeira Gabellini et al. 2019), τ_ν is assessed at larger than 30, which corresponds to the optically thick disk. We note that current ALMA observations reported lower κ per unit dust mass (~100 cm^2 g^{-1} at near-IR; Birnstiel et al. 2018). With this value τ_ν is estimated as 3.75 and is enough for the optically thick disk.

With the temperature of 202.5 K, the disk aspect ratio ($H/r_{\rm spiral}$) at the location of the spiral structure is estimated to be 0.15. Here, $H = c_s/\Omega_{\rm K}$ is the disk scale height, where c_s and $\Omega_{\rm K}$ are the sound speed and the Keplerian angular velocity, respectively.

3.2. Scattering

We then investigate whether both of the results taken by Subaru/HiCIAO and Keck/NIRC2 can be reproduced by only scattering. As a rough estimate of the surface brightness of the scattered light, we use Equation (9) in Inoue et al. (2008), which is an approximate analytic expression of the scattered light (D'Alessio et al. 1999, 2006). With the modification for inclined disks (see also Jang-Condell & Turner 2013), the observable intensity is given by

$$I_\nu^{\rm sca} \simeq \beta\omega_\nu H(1,\omega_\nu)B_\nu(T_\star)\frac{\Omega_\star}{4\pi}\frac{1}{\sin\beta+\cos\eta}, \quad (2)$$

where β, ω_ν, $\Omega_\star = \pi\frac{R_\star^2}{r_{\rm spiral}^2}$, and $T_\star$ are a grazing angle, albedo, a solid angle of the stellar photosphere from the spiral, and effective temperature of CQ Tau, respectively. η is defined as the sum of the inclination and $\arctan(\frac{dH(r)}{dr}) \sim H/r$. $H(1,\omega_\nu)$ represents the law of diffuse reflection (Chandrasekhar 1960) and $B_\nu(T_\star)$ is Planck's law. Here, we assume $H(1,\omega_\nu) = 1$ (single scattering) for simplicity.[32]

To estimate the surface brightness of the scattered light from the spiral region, we used the disk and dust parameters estimated in Section 3.1. With this dust model, the albedo is about 0.4 at the H band. The grazing angle ($\beta = dH/dr - \arctan(H/r) = f \times H/r$, where f is a flaring index defined by $H(r) \propto r^{(1+f)}$) is assumed to be $\beta \lesssim H/r = 0.15$ ($f \lesssim 1$). $R_\star$ was derived from the Stefan–Boltzmann law with $T_\star = 6900$ K and $L_\star = 10L_\odot$ (Testi et al. 2001; Ubeira Gabellini et al. 2019). We used 50 au as a typical value for $r_{\rm spiral}$ and $i = 35°$ for the disk's inclination (Ubeira Gabellini et al. 2019). We finally assessed the expected scattered brightness as 62 and 8.5 mJy arcsec^{-2} at the H and L' band, respectively. Note that we do not take into account of polarization degree in the H-band calculation. In the HiCIAO result, the spiral has a surface brightness of ~30–40 mJy arcsec^{-2} and does not show a large disagreement with the estimate. The NIRC2 result, however, is much brighter than the expected brightness in the L' band.

We note that CQ Tau has IR excess in its spectral energy distribution (Ubeira Gabellini et al. 2019). The inner disk with an effective temperature of ~1000 K may behave as another source of heating and scattering mechanisms at the L' band. Assuming that the inner disk contributes as the light source of the scattering more than the central star by an order of magnitude, the expected L'-band brightness of the spiral is ~90 mJy arcsec^{-2} and is comparable to the NIRC2 result. Therefore, both thermal emission and scattering may equally contribute to the spiral feature at the L' band, if the disk is heated up to ~200 K at ~50 au and the inner part of the disk contributes as a light source of scattering. Detailed discussions using radiative transfer modeling will help to have better understandings of the spiral feature.

3.3. Formation Scenario of the Spiral

We have seen that the disk temperature at ~50 au can be ~200 K, indicating that the disk aspect ratio is ~0.15. The pitch angle of the spiral feature (in radian) is comparable with the disk aspect ratio if the spiral feature is due to the spiral density wave in a differentially rotating disk (e.g., Rafikov 2002; Bae & Zhu 2018). However, the fitted pitch angle of the spiral from the r^2-scaled HiCIAO image (34° ± 2°) is much larger than the expected $H/r_{\rm spiral} = 0.15$. Tang et al. (2017) reported a large pitch angle in the AB Aur disk, which is similar to the CQ Tau case, and they predicted an unseen gaseous planet that coincides with the large pitch angle. As mentioned in Section 1, a high-mass planet can induce shocks and heat the spiral enough to be detected in the L' band (Lyra et al. 2016). The heating of the spiral arms driven by a massive companion may occur due to shock heating (⩽15°–20°; Dong et al. 2015b; Zhu et al. 2015). In this sense the prediction of Ubeira Gabellini et al. (2019) of an unseen protoplanet is consistent with a heated spiral scenario.

Several other mechanisms can induce a large pitch angle: gravitational instability (⩽15°–20°; Dong et al. 2015a) or shadow casting (⩽20°–25°; Montesinos et al. 2016; Montesinos & Cuello 2018). Note that these studies, in many cases, assume a vertically isothermal disk temperature profile. Juhász & Rosotti (2018) performed another simulation by assuming that the disk surface is hotter than the midplane and showed that the spiral pitch angle near the surface can be more open compared to that at disk midplane. As we mentioned in Section 2.2, our fitted result of the pitch angle can be distorted by the inclination effect and we do not identify the mechanism to make a wide-open spiral. Combining gas observations of different emission lines enables to estimate the vertical temperature profile of the disk (Akiyama et al. 2011, 2013) and such future observations will help to understand the thermal structure of the spiral. Since the NIRC2 observation did not detect any companion candidates, follow-up observations to search for planets within 30 au are required to further investigate this scenario.

4. Conclusion

We have newly detected a spiral in the CQ Tau disk using the Keck/NIRC2 L'-band imaging and Subaru/AO188 +HiCIAO H-band polarimetric imaging observations. The spiral feature overlaps with the ring structure in the ALMA continuum and is consistent with a prediction of a Jovian protoplanet at 20 au (Ubeira Gabellini et al. 2019). However, our observations did not confirm the presence of the gap reported by the ALMA observations. We did not detect any companion candidates within 0.″9 from the central star either. The 5σ contrast limit could constrain down to ~5 $M_{\rm J}$ though it is affected by the spiral structures at separations of 0.″2–0.″4. We traced peaks of the spiral in the r^2-scaled HiCIAO image to derive a pitch angle of the spiral (34° ± 2°). This fitted result is also used for forward modeling to reproduce the ADI-reduced NIRC2 image and we estimated the original surface brightness in the L' band to be ~126 mJy arcsec^{-2} at most.

We have investigated whether the L'-band emission can be reproduced by thermal emission. The observed emission of 126 mJy arcsec^{-2} corresponds to the brightness temperature of ~202.5 K. The temperature of dust grains at the spiral location can be ~200 K if the grain size is ~0.8 μm and the albedo is ~0.2 for an astronomical silicate model (Draine & Lee 1984). The H-band emission originates from the scattering from the disk surface while both scattering and thermal emission may contribute to the L'-band emission, depending on the condition of the inner disk.

Follow-up observations for the disk exploration as well as the companion search will help to understand this bright spiral feature. The L'-band profile for the spiral feature may be improved by high-contrast imaging with RDI. PDI observations with an updated AO instrument such as Subaru/SCExAO, Gemini/GPI,

[32] For a multiscattering case, see also Equation (9) in Jang-Condell & Turner (2013).

or Very Large Telescope/SPHERE will also be able to provide clearer images of the disk, which helps to understand the disk characteristics by spatially resolving the spiral. Combining gas observations of different emission lines enables the estimation of the vertical temperature profile of the disk.

The authors would like to thank the anonymous referees for the constructive comments and suggestions to improve the quality of the paper. We wish to thank Mitsuhiko Honda for constructive comments to improve our discussions with the NIRC2 result. Some of the data presented herein were obtained at the W. M. Keck Observatory, which is operated as a scientific partnership among the California Institute of Technology, the University of California, and the National Aeronautics and Space Administration. The Observatory was made possible by the generous financial support of the W. M. Keck Foundation. A part of this research is based on data collected at the Subaru Telescope, which is operated by the National Astronomical Observatories of Japan. Based in part on data collected at Subaru telescope and obtained from the SMOKA, which is operated by the Astronomy Data Center, National Astronomical Observatory of Japan. This paper makes use of the following ALMA data: ADS/JAO.ALMA#2017.1.01404.S. ALMA is a partnership of ESO (representing its member states), NSF (USA) and NINS (Japan), together with NRC (Canada), *MOST* and ASIAA (Taiwan), and KASI (Republic of Korea), in cooperation with the Republic of Chile. The Joint ALMA Observatory is operated by ESO, AUI/NRAO, and NAOJ. This research has made use of NASA's Astrophysics Data System Bibliographic Services. This research has made use of the SIMBAD database, operated at CDS, Strasbourg, France. This research has made use of the VizieR catalog access tool, CDS, Strasbourg, France. The original description of the VizieR service was published in Ochsenbein et al. (2000).

T.U. acknowledges JSPS overseas research fellowship. This work was supported by MEXT/JSPS KAKENHI grant Nos. 15H02063, 17K05399, 18H05442, 19H00703, 19H05089, and 19K03932. Part of this work was carried out at the Jet Propulsion Laboratory, California Institute of Technology, under contract with the National Aeronautics and Space Administration (NASA). The material is based upon work supported by NASA under award No. 80NSSC19K0294. The research leading to these results has received funding from the European Research Council under the European Union's Seventh Framework Program (ERC grant Agreement no. 337569) and Horizon 2020 Research and Innovation Program (grant agreement No. 819155), and from the Wallonia-Brussels Federation (grant for Concerted Research Actions). V.C. acknowledges funding from the Australian Research Council via DP180104235. O.A. acknowledges funding from FRS-FNRS. J.B. acknowledges support by NASA through the NASA Hubble Fellowship grant #HST-HF2-51427.001-A awarded by the Space Telescope Science Institute, which is operated by the Association of Universities for Research in Astronomy, Incorporated, under NASA contract NAS5-26555.

The authors wish to acknowledge the very significant cultural role and reverence that the summit of Maunakea has always had within the indigenous Hawaiian community. We are most fortunate to have the opportunity to conduct observations from this mountain.

Appendix
Supplementary Keck/NIRC2 Images

We present supplementary images to clearly show our Keck/NIRC2 result. Figure 7 presents a set of different PCs. Figure 8 shows the NIRC2 results superimposed with the ALMA continuum (left) and a full FoV version of the VIP-ADI reduction (right). Figure 9 shows the best-fit Archimedean spirals ($r = a + b \times \theta^n$) that reproduce well the observed features (left for the

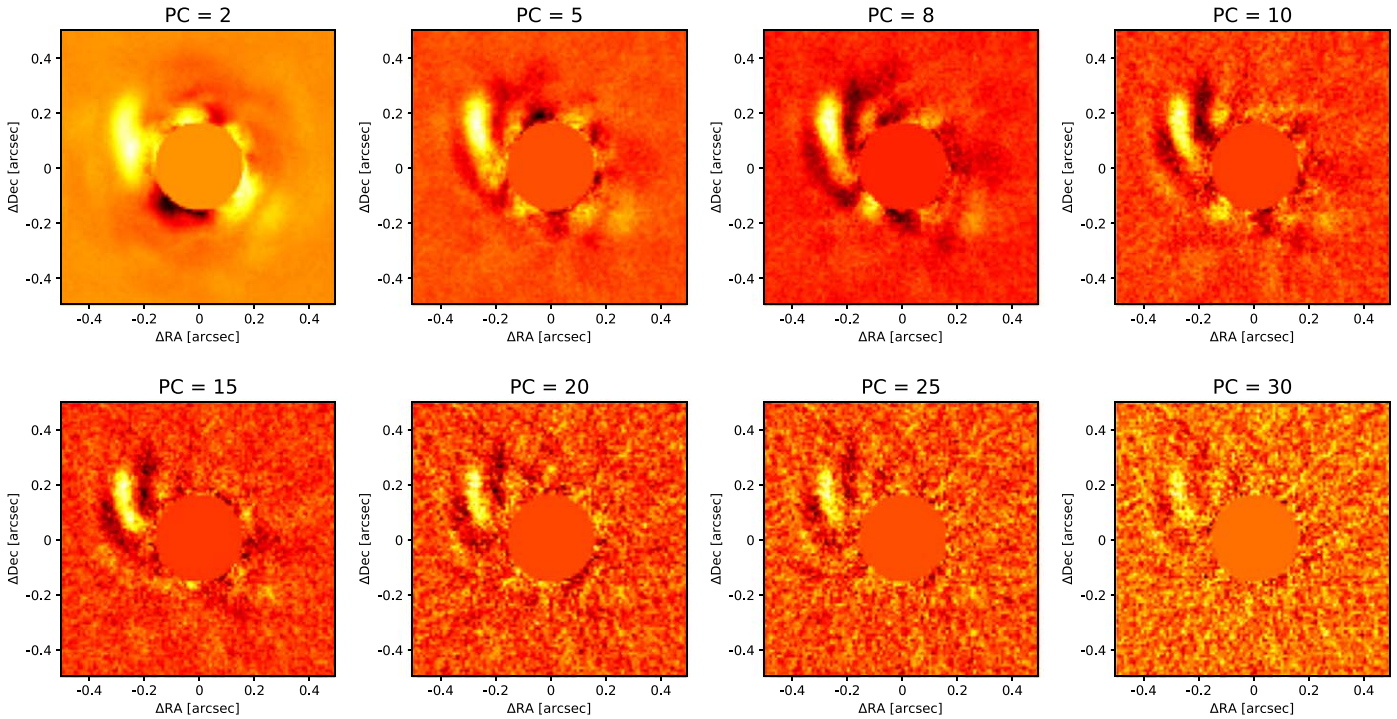

Figure 7. Keck/NIRC2 ADI-reduced images of CQ Tau at different PCs. These images also detected the same spiral structure with S/Ns > 5.

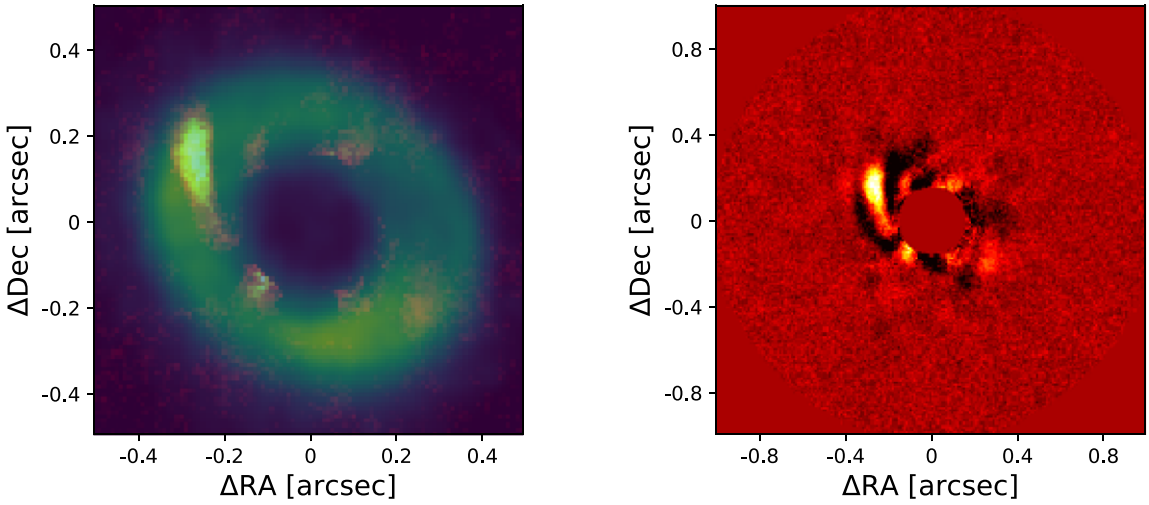

Figure 8. Left: the same as Figure 1, superimposed with the ALMA continuum (yellow–green). Right: ADI-reduced NIRC2 image (PC = 8) with a larger FoV.

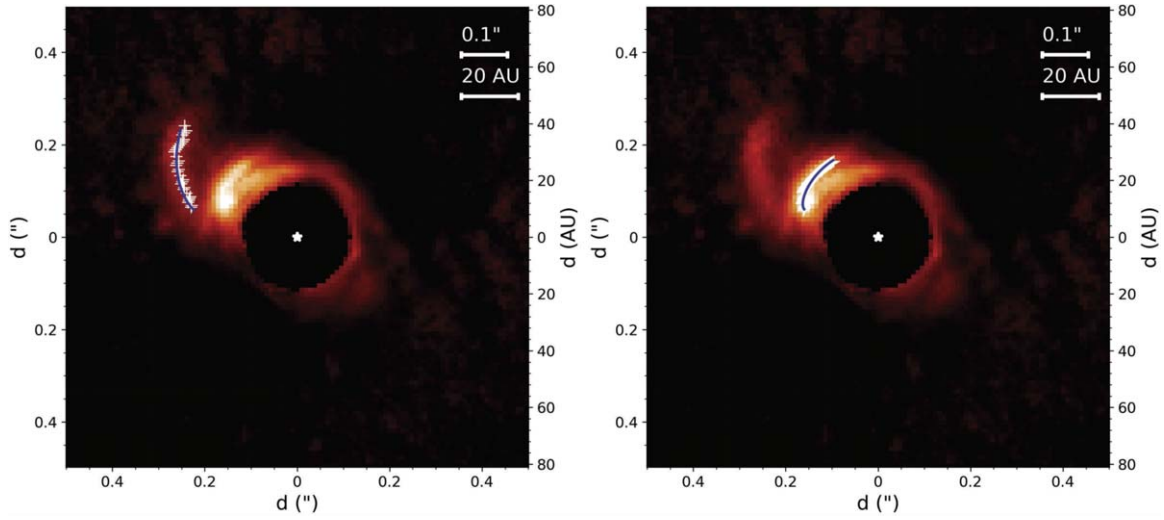

Figure 9. Same as the middle and right panels in Figure 4 for the fitted result with the best-fit general Archimedean spirals.

outer spiral: $a = 0.''221 \pm 0.''004$, $b = 0.''203 \pm 0.''010$, $n = 0.744 \pm 0.045$; right for the inner feature: $a = 0.''141 \pm 0.''006$, $b = 0.''056 \pm 0.''007$, $n = 0.149 \pm 0.079$).

ORCID iDs

Taichi Uyama https://orcid.org/0000-0002-6879-3030
Dimitri Mawet https://orcid.org/0000-0002-8895-4735
Jun Hashimoto https://orcid.org/0000-0002-3053-3575
Tomoyuki Kudo https://orcid.org/0000-0002-9294-1793
Garreth Ruane https://orcid.org/0000-0003-4769-1665
Olivier Absil https://orcid.org/0000-0002-4006-6237
Eiji Akiyama https://orcid.org/0000-0002-5082-8880
Jaehan Bae https://orcid.org/0000-0001-7258-770X
Michael Bottom https://orcid.org/0000-0003-1341-5531
Elodie Choquet https://orcid.org/0000-0002-9173-0740
Thayne Currie https://orcid.org/0000-0002-7405-3119
Ruobing Dong https://orcid.org/0000-0001-9290-7846
Katherine B. Follette https://orcid.org/0000-0002-7821-0695
Misato Fukagawa https://orcid.org/0000-0003-3500-2455
Jungmi Kwon https://orcid.org/0000-0003-2815-7774
Satoshi Mayama https://orcid.org/0000-0002-3424-6266
Tiffany Meshkat https://orcid.org/0000-0001-6126-2467
Maddalena Reggiani https://orcid.org/0000-0003-2911-0898
Motohide Tamura https://orcid.org/0000-0002-6510-0681
Leonardo Testi https://orcid.org/0000-0003-1859-3070
Nicole Wallack https://orcid.org/0000-0003-0354-0187
Jonathan Williams https://orcid.org/0000-0001-5058-695X
Zhaohuan Zhu https://orcid.org/0000-0003-3616-6822

References

Akiyama, E., Momose, M., Hayashi, H., & Kitamura, Y. 2011, PASJ, 63, 1059
Akiyama, E., Momose, M., Kitamura, Y., et al. 2013, PASJ, 65, 123
ALMA Partnership, Brogan, C. L., Pérez, L. M., et al. 2015, ApJL, 808, L3
Amara, A., & Quanz, S. P. 2012, MNRAS, 427, 948
Andrews, S. M., Huang, J., Pérez, L. M., et al. 2018, ApJL, 869, L41
Bae, J., & Zhu, Z. 2018, ApJ, 859, 119
Baraffe, I., Chabrier, G., Barman, T. S., Allard, F., & Hauschildt, P. H. 2003, A&A, 402, 701
Benisty, M., Juhasz, A., Boccaletti, A., et al. 2015, A&A, 578, L6
Birnstiel, T., Dullemond, C. P., Zhu, Z., et al. 2018, ApJL, 869, L45
Chandrasekhar, S. 1960, Radiative Transfer (New York: Dover)
Chapillon, E., Parise, B., Guilloteau, S., Dutrey, A., & Wakelam, V. 2010, A&A, 520, A61
Christiaens, V., Casassus, S., Absil, O., et al. 2019, MNRAS, 486, 5819

Currie, T., Cloutier, R., Brittain, S., et al. 2015, ApJL, 814, L27
D'Alessio, P., Calvet, N., Hartmann, L., Franco-Hernández, R., & Servín, H. 2006, ApJ, 638, 314
D'Alessio, P., Calvet, N., Hartmann, L., Lizano, S., & Cantó, J. 1999, ApJ, 527, 893
Dong, R., Fung, J., & Chiang, E. 2016, ApJ, 826, 75
Dong, R., Hall, C., Rice, K., & Chiang, E. 2015a, ApJL, 812, L32
Dong, R., Liu, S.-Y., Eisner, J., et al. 2018a, ApJ, 860, 124
Dong, R., Najita, J. R., & Brittain, S. 2018b, ApJ, 862, 103
Dong, R., Zhu, Z., Rafikov, R. R., & Stone, J. M. 2015b, ApJL, 809, L5
Draine, B. T., & Lee, H. M. 1984, ApJ, 285, 89
Gaia Collaboration, Brown, A. G. A., Vallenari, A., et al. 2018, A&A, 616, A1
Ginski, C., Stolker, T., Pinilla, P., et al. 2016, A&A, 595, A112
Gomez Gonzalez, C. A., Wertz, O., Absil, O., et al. 2017, AJ, 154, 7
Hashimoto, J., Dong, R., Kudo, T., et al. 2012, ApJL, 758, L19
Hashimoto, J., Tamura, M., Muto, T., et al. 2011, ApJL, 729, L17
Huang, J., Andrews, S. M., Pérez, L. M., et al. 2018, ApJL, 869, L43
Inoue, A. K., Honda, M., Nakamoto, T., & Oka, A. 2008, PASJ, 60, 557
Jang-Condell, H., & Turner, N. J. 2013, ApJ, 772, 34
Juhász, A., & Rosotti, G. P. 2018, MNRAS, 474, L32
Keppler, M., Benisty, M., Müller, A., et al. 2018, A&A, 617, A44
Kraus, S., Kreplin, A., Fukugawa, M., et al. 2017, ApJL, 848, L11
Kuhn, J. R., Potter, D., & Parise, B. 2001, ApJL, 553, L189
Lyra, W., Richert, A. J. W., Boley, A., et al. 2016, ApJ, 817, 102
Marois, C., Macintosh, B., Barman, T., et al. 2008, Sci, 322, 1348
Mawet, D., Choquet, É, Absil, O., et al. 2017, AJ, 153, 44
McDonald, I., Zijlstra, A. A., & Watson, R. A. 2017, MNRAS, 471, 770
Milli, J., Mouillet, D., Lagrange, A. M., et al. 2012, A&A, 545, A111
Montesinos, M., & Cuello, N. 2018, MNRAS, 475, L35
Montesinos, M., Perez, S., Casassus, S., et al. 2016, ApJL, 823, L8
Muto, T., Grady, C. A., Hashimoto, J., et al. 2012, ApJL, 748, L22
Natta, A., Prusti, T., Neri, R., et al. 2001, A&A, 371, 186
Ochsenbein, F., Bauer, P., & Marcout, J. 2000, A&AS, 143, 23
Ohta, Y., Fukagawa, M., Sitko, M. L., et al. 2016, PASJ, 68, 53
Pérez, L. M., Carpenter, J. M., Andrews, S. M., et al. 2016, Sci, 353, 1519
Pinte, C., Price, D. J., Ménard, F., et al. 2018, ApJL, 860, L13
Rafikov, R. R. 2002, ApJ, 569, 997
Rameau, J., Chauvin, G., Lagrange, A. M., et al. 2012, A&A, 546, A24
Reggiani, M., Christiaens, V., Absil, O., et al. 2018, A&A, 611, A74
Ruane, G., Ngo, H., Mawet, D., et al. 2019, AJ, 157, 118
Serabyn, E., Huby, E., Matthews, K., et al. 2017, AJ, 153, 43
Soummer, R., Pueyo, L., & Larkin, J. 2012, ApJL, 755, L28
Strom, K. M., Strom, S. E., Edwards, S., Cabrit, S., & Skrutskie, M. F. 1989, AJ, 97, 1451
Tamura, M. 2009, in AIP Conf. Ser. 1158, Exoplanets and Disks: Their Formation and Diversity, ed. T. Usuda, M. Tamura, & M. Ishii (Melville, NY: AIP), 11
Tang, Y.-W., Guilloteau, S., Dutrey, A., et al. 2017, ApJ, 840, 32
Testi, L., Natta, A., Shepherd, D. S., & Wilner, D. J. 2001, ApJ, 554, 1087
Tsukagoshi, T., Muto, T., Nomura, H., et al. 2019, ApJL, 878, L8
Ubeira Gabellini, M. G., Miotello, A., Facchini, S., et al. 2019, MNRAS, 486, 4638
Uyama, T., Hashimoto, J., Kuzuhara, M., et al. 2017, AJ, 153, 106
Uyama, T., Hashimoto, J., Muto, T., et al. 2018, AJ, 156, 63
van der Marel, N., van Dishoeck, E. F., Bruderer, S., et al. 2013, Sci, 340, 1199
Wagner, K., Stone, J. M., Spalding, E., et al. 2019, ApJ, 882, 20
Xuan, W. J., Mawet, D., Ngo, H., et al. 2018, AJ, 156, 156
Zhu, Z., Dong, R., Stone, J. M., & Rafikov, R. R. 2015, ApJ, 813, 88